An ERS-1 Synthetic Aperture Radar Image of a Tropical Squall Line Compared with Weather Radar Data

I-I. Lin, Werner Alpers, *Member, IEEE*, Victor Khoo, Hock Lim, *Member, IEEE*, Tian Kuay Lim, and Dayalan Kasilingam, *Member, IEEE*

***Abstract*—A radar image acquired by the C-band synthetic aperture radar (SAR) aboard the European Remote Sensing satellite ERS-2 over the coastal waters south of Singapore showing radar signatures of a strong tropical squall line ("Sumatra Squall") is compared with coincident and collocated weather radar data. Squall line features such as the gust front, areas of updraft convergence, and rain areas are identified. Possible attenuation effects from the rain drops in the atmosphere under very heavy rain (rain rate $>$ 100 mm/h) is suggested. In addition, the possibility of extracting the associated geophysical parameters, i.e., rain rate and wind speed from SAR imagery is investigated. The rain rate is estimated from the attenuation signature in the SAR image. Comparison between the estimated rain rate and weather radar rain rate shows consistency. Wind speed associated with the squall line is estimated based on the CMOD4 wind scatterometer model. The estimated wind speed pattern appears to be in agreement with the observed squall line structure. Possible errors in the wind estimation due to effects of rain are suggested.**

I. Introduction

PRECIPITATION in the tropics usually occurs in the form of intermittent rain events, also called rain cells, which are strongly localized in time and space. They are categorized into four different groups: 1) ordinary storm cells (also called "ordinary rain cells"), 2) supercell storms, 3) multicell storms, and 4) squall lines [1], [2]. Tropical rain cells consist of convective clouds (cumulonimbus clouds or thunderstorms) which are the source of heavy rain and lightning in the equatorial regions. Ever since the SEASAT mission in 1978, radar signatures of tropical rain cells have been observed on synthetic aperture radar (SAR) images acquired over tropical ocean [3]–[12]. Quantitative investigations of these radar signatures have been hampered by the lack of *in-situ* measurements for comparison. To a large extent, the interpretation still remains speculative. Though the potential of using ground or ship-based weather radar data for comparison with SAR images showing radar signatures of rain cells has long been recognized, only very few cases have been reported where such coincident and collocated data sets are available [5]–[7], [12].

SAR images from the European Remote Sensing satellites ERS-1 and ERS-2, which have been acquired over tropical oceans, often show radar signatures of all four types of rain cells. This SAR operates at a frequency of 5.3 GHz (C-band) and at vertical polarization for transmission and reception (VV polarization). The swath width is 100 km and the incidence angle lies between 20.10° and 25.9°. In this paper, we present an ERS-2 SAR image which was acquired over coastal waters south of Singapore on September 22, 1996 and which shows radar signatures of a tropical squall line with very heavy precipitation (in some areas larger than 125 mm/h). Such strong tropical squall lines are often encountered in the Strait of Malacca separating the Malay Peninsula from the Indonesian island of Sumatra. Since these squall lines have their origin in Sumatra they are also called "Sumatra Squalls." In our analysis of the ERS-2 SAR image of September 22, 1996 we incorporate for comparison two sets of radar data which were acquired by two ground-based weather radars located in Singapore. It turns out that they greatly assist in feature identification and validation of the analysis of the ERS-2 SAR image.

The possibility of using SAR backscatter signatures quantitatively in extracting the associated geophysical parameters of rain events is discussed. Possible areas of attenuation in the SAR backscatter by heavy rainfall are suggested. These signatures are investigated further to estimate the associated rain rate based on the attenuation relationship for C-band radar by tropical. In addition, the SAR backscatter signatures are used to estimate wind speed across the squall line. This possibility in estimating wind speed in the SAR imagery using scatterometry models has received considerable attention in the recent literature [13]–[19]. Given the wind direction, the wind speed can be estimated from the single backscatter measurement of SAR by using a wind scatterometer model, e.g., the CMOD 4 model [20], [21]. This concept of using SAR as a high-resolution wind mapper has shown to be useful in providing detail wind structures of specific mesoscale atmospheric phenomena and is applied here in revealing detail wind structures of the tropical squall lines.

Manuscript received January 26, 2000; revised January 2, 2001.

I.-I. Lin is with the National Center for Ocean Research, Institute of Oceanography, National Taiwan University, Taipei, Taiwan, R.O.C.

H. Lim and V. Khoo are with the Centre for Remote Imaging, Sensing and Processing (CRISP), Faculty of Science, National University of Singapore, Singapore 119260 (e-mail: crslinii@leonis.nus.edu.sg).

W. Alpers is with the Institut fuer Meereskunde, Universitaet Hamburg, D-22529 Hamburg, Germany (e-mail: alpers@ifm.uni-hamburg.de).

T. K. Lim is with the Meteorological Service Singapore, Singapore Changi Airport, Singapore 918141 (e-mail: mssltk@pacific.net.sg).

D. Kasilingam is with the Department of Electrical and Computer Engineering, University of Massachusetts, Dartmouth, North Dartmouth, MA 02747-2300 USA (e-mail: dkasilingam@umassd.edu).

Publisher Item Identifier S 0196-2892(01)04015-3.

II. Tropical Squall Lines

Meteorologist usually define a squall line as a line of thunderstorms [1]. A tropical squall line is associated strong convective activity and consists of clusters of rain cells whose physical dimension can be several hundred kilometers. The individual rain cells tend to be aligned at the forefront of the squall line. Since the associated wind gust fronts of the individual rain cells usually merge to form a single gust line, it seems to be appropriate to call such rain event squall line.

"Sumatra Squalls" are tropical squall lines or thunderstorms that affect the Malay Peninsula and Singapore. During the colonial period (before 1962), the British meteorologists at the forecast offices in this region called this special type of thunderstorms "Sumatra Squalls" because they believed that they have their origin at the island of Sumatra. Later weather satellite observations have shown that the Sumatra Squalls are often triggered by the arrival of equatorial super clusters of thunderstorms (a component of the Madden–Julian oscillation) that propagate into the region from across the Indian Ocean (from the crest).

Weather radar images have revealed that the development of a Sumatra Squall starts with strong convective activities in the Malacca Strait during the night. Individual rain cells begin bubbling up in the Strait of Malacca from about 2000 local time. As the convective cells grow more widespread and intense, they align themselves into a line, sometimes extending more than 300 km from south to north. During the night, the line of thunderstorms are held off the west coast of the Malay Peninsula, probably by land breeze. During sunrise, they sweep in over land, generating in the early morning hours strong gusts and heavy showers in Singapore and the southern region of Malaysia.

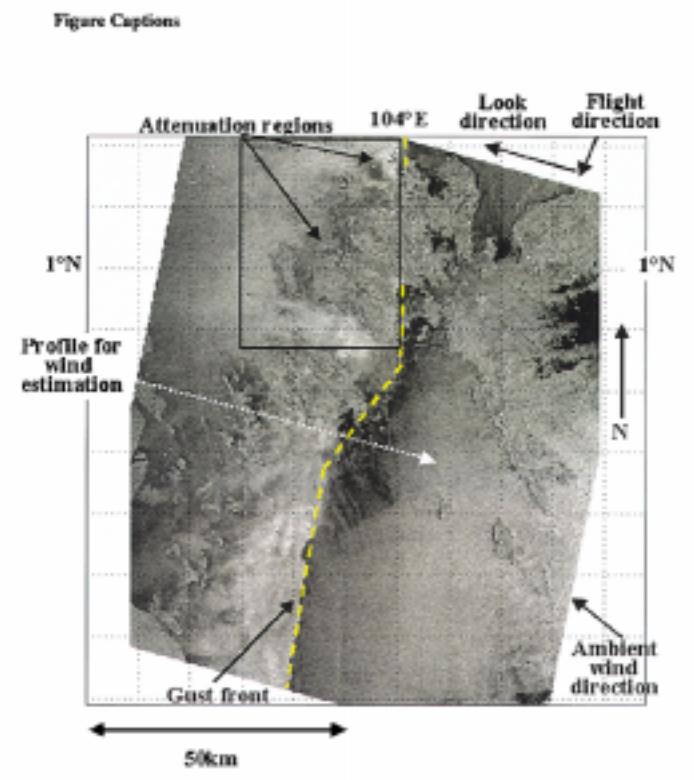

Fig. 1. ERS-2 SAR image of a squall line ("Sumatra Squall") located over the coastal waters south of Singapore (orbit: 07444, frame: 3591, date: September 22, 1996, time: 0324 UTC). The box-marked area in the upper part of the SAR image denotes the area which was also imaged by the Singapore C-band weather radar one minute later (see Fig. 7). The gust front associated with the squall line propagating southeastwards is marked by a dashed line. Also inserted in this image is the profile (dotted line) along which the windspeed is determined.

III. ERS SAR Images

Fig. 1 shows an ERS-2 SAR image of an ocean area south of Singapore on which radar signatures of a tropical squall line (Sumatra Squall) can be delineated. This image was acquired on September 22, 1996 at 0324 UTC or 1124 local time during a descending pass of the ERS-2 satellite (orbit: 07444, frame: 3591, center coordinates: 0.752 N, 103.938 E). In order to facilitate the comparison with the weather radar data we have displayed this SAR image in Fig. 1 as an equidistant cylindrical map projection. In this SAR image we have marked the gust front of the squall line by a dashed line. As can be seen on the ERS-2 SAR image acquired over the adjacent southern area (same orbit, but frame 3609, not shown here), the frontal line extends approximately 80 km further south. The box inserted into the image of Fig. 1 marks the area for which a detailed comparison with weather radar data will be carried out in Section V. The dashed line inserted in the SAR image denotes a profile along which the variation of the normalized radar cross section (NRCS) will be determined and converted into wind speed. Another ERS-2 SAR image of the same ocean area, which was acquired on January 10, 1999 at 0324 UTC (orbit: 19468, frame: 3591) is depicted in Fig. 2 for comparison. On this day there was no squall line present and the islands in the Strait of Singapore were not obscured by rain cells. The comparison of both images clearly

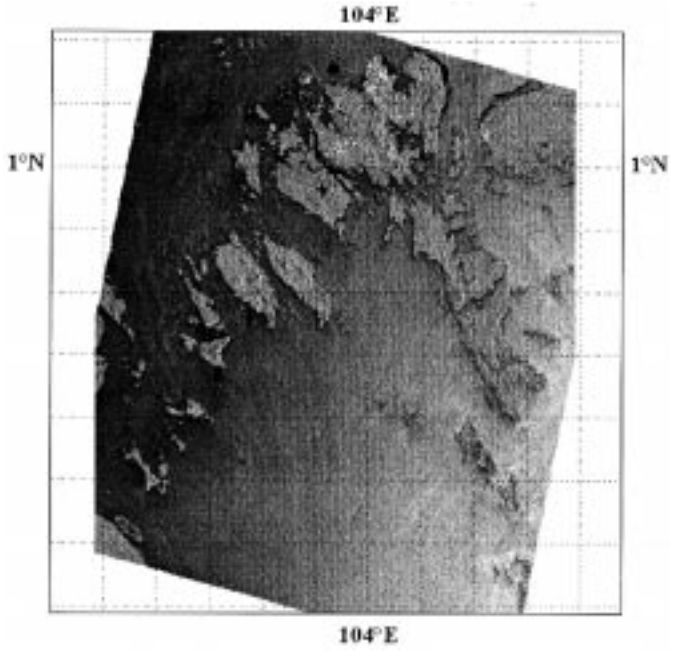

Fig. 2. ERS-2 SAR image of the same area as in Fig. 1, but acquired on a clear day when there was no squall line present (orbit: 19468, frame: 3591, date: January 10, 1996, time: 0324 UTC). Visible are the islands in the Strait of Singapore which were obscured in the ERS-2 SAR image depicted in Fig. 1 by the presence of the squall line.

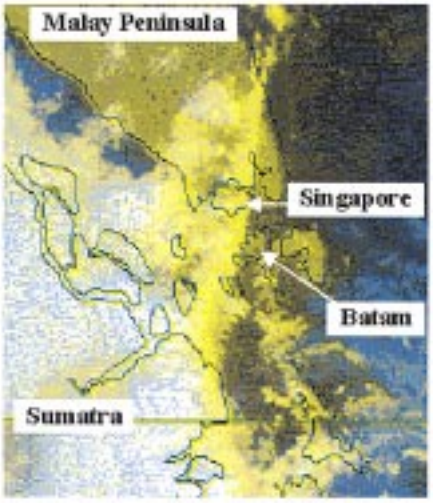

Fig. 3. Image acquired in the visible band by the Japanese weather satellite GMS on September 22, 1996 at 0230 UTC showing a cloud front extending north to south from the east coast of the Malay Peninsula, via the east coast of Singapore to the east coast of Sumatra. The position of this cloud front is close to the position of the gust line visible on the ERS-2 SAR image depicted in Fig. 1.

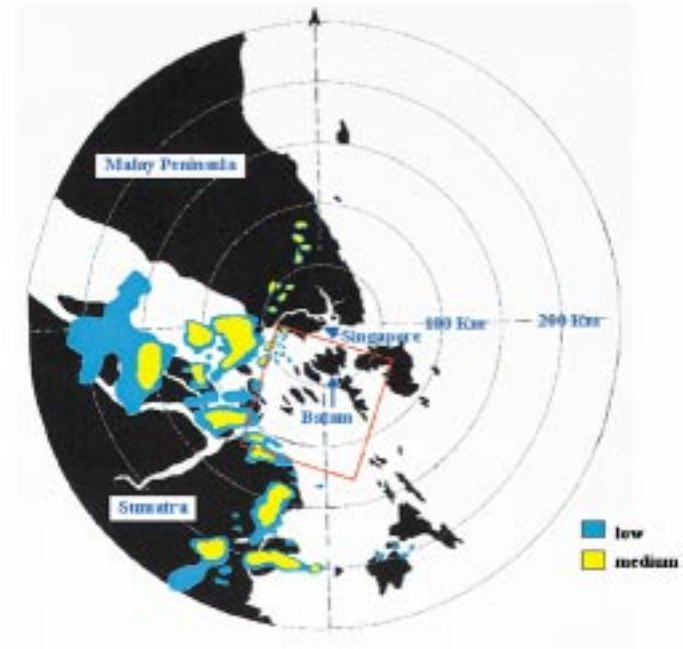

Fig. 4. Color-coded plot of radar reflectivity derived from data of the S-band weather radar located at Singapore which were acquired on September 22, 1996 at 0200 UTC, i.e., 1 h and 24 min before the acquisition of the SAR image depicted in Fig. 1. The color code is such that red denotes high, yellow medium, and blue low radar reflectivity corresponding to high, medium, and low rain rate, respectively. The circles denote the 50, 100, 150, 200, and 250 km range isolines.

shows that for the strong rain event of September 22 the attenuation of the microwaves by the rain drops in the atmosphere affects the radar signature over water as well as over land.

IV. Comparison with a Weather Satellite Image

First we compare the SAR image depicted in Fig. 1 with an image acquired in the visible band by the Japanese Geostationary Meteorological Satellite (GMS), on September 22, 1996 at 0230 UTC, i.e., 54 min. before the acquisition of the ERS-2 SAR image. (Unfortunately, the satellite image of 0330 UTC is not available because of transmission problems.) This image, which is depicted in Fig. 3, shows a cloud front extending north-south from the east coast of the Malay Peninsula via the east coast of Singapore to the east coast of Sumatra. The position of the cloud front is perspicuous close to the position of the gust front visible on the SAR image (Fig. 1). The fact that the position of the cloud front visible on the GMS image is slightly west of the position of the frontal line visible on the SAR is due to the fact that the squall line was moving southeastwards. This motion can be inferred, e.g., from the observation that the position of the gust front in the ERS SAR image which was acquired at 0324 UTC lies between the position of the cloud front in the GMS images acquired at 0230 UTC and 0430 UTC (not reproduced here). In addition, also the comparison of the position of the cloud front in the GMS images acquired at 0030 UTC, 0130 UTC, 0230 UTC, and 0430 UTC (not reproduced here) clearly reveals a southeastward motion of the cloud front.

V. Comparison with Weather Radar Images

Evidence that the radar signatures visible in the left-hand section of the SAR image originate indeed from a tropical squall line is provided by radar images from two ground-based weather radar stations in Singapore. The first weather radar is an incoherent S-band radar operating at horizontal polarization for transmission and reception. From the data of this radar hand-plotted images are produced every hour from the display on the plane position indicator (PPI) screen. For ranges below 100 km, the radar reflectivity data are averaged over the elevation angles from 6 to 20°, and for ranges beyond 100 km (maximum range: 400 km) the radar reflectivity data are recorded from the elevation angle of 1°. The radar reflectivity is recorded only at three levels (level 1: $<$8 dB, level 2: 8–32 dB, level 3: $>$32 dB). Although these hand-plotted images cannot be used for estimating rain rates, they do yield valuable information on the spatial and temporal evolution of the squall line.

Figs. 4–6 show three of these hand-plotted images derived from the S-band weather radar data which were acquired on September 22, 1996 at 0200, 0300, and 0400 UTC, respectively. The box inserted in the images marks the location of the ERS-2 SAR scene depicted in Fig. 1 which covers an area of 100 km $\times$ 100 km. These plots reveal that the areal extent of the Sumatra Squall is approximately 300 km and that, within two hours, its shape varies considerably. From the first plot (Fig. 4) we see that the Sumatra Squall has its origin in the northern part of Sumatra. By comparing the three plots we see that the front of the squall line was moving southeastwards with a speed of approximately 30 km/h, which is consistent with the speed that we have estimated also from successive GMS images. An interesting observation is that the region of high reflectivity and thus of high precipitation (red region) just south of Singapore visible in the weather radar images of 0300 UTC (Fig. 5) and 0400 UTC (Fig. 6) have hardly moved during one hour.

In Fig. 5, the position of the gust front visible on the ERS-2 SAR (Fig. 1) is marked by a red solid line. It can be seen that the

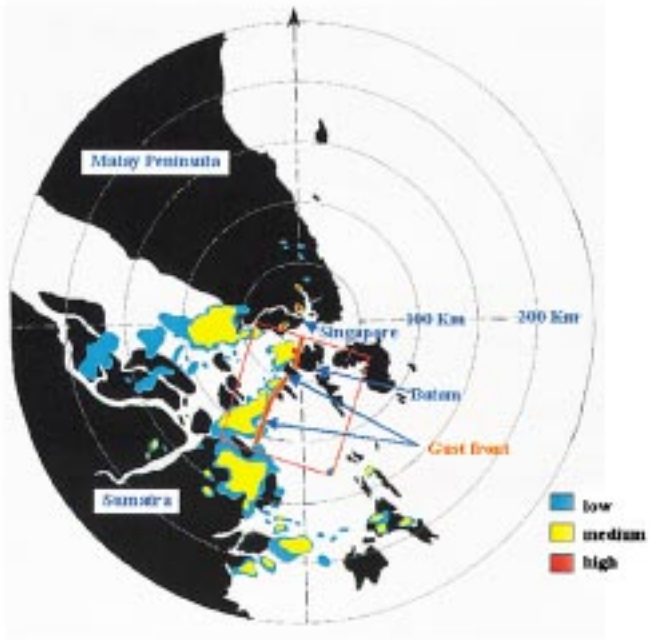

Fig. 5. Same plot as in Fig. 3, but acquired at 0300 on the same day, i.e., 36 min before the acquisition of the SAR image depicted in Fig. 1. Comparison of this plot with the one of Fig. 4 reveals that the squall line was propagating south eastwards.

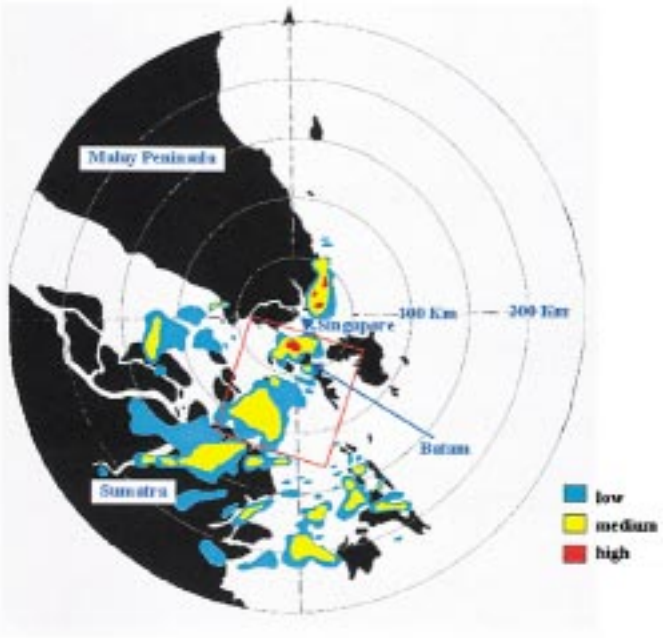

Fig. 6. Same plot as in Fig. 3, but acquired at 0400 UTC on the same day, i.e., 96 minutes after the acquisition of the SAR image depicted in Fig. 1. Note that the region of heavy rainfall south of Singapore (red blob in Figs. 5 and 6) has hardly moved, whereas the front line has moved south eastwards with a speed of approximately 30 km/h.

position of the gust front correlates quite well with the position of the frontal boundary of the squall line on the weather radar image. Note, however, that there is a time difference of 24 min between the two data acquisitions and thus no exact collocation can be expected.

Further evidence of the existence of the tropical squall line is obtained from the second weather radar located in Singapore, which is a C-band (5.6 GHz) Doppler radar (model DWSR-88C) manufactured by Enterprise Electronics Corporation (Alabama, USA). It operates also at horizontal polarization for transmission and reception, and its antenna has a beamwidth of 1°. Although this is a Doppler radar, only the radar reflectivity data from a range up to 60 km are recorded digitally. From the reflectivity data the reflectivity factor is derived which is then converted into rain rate (see Appendix A). The reflectivity factor is measured every 5 min. Six levels of reflectivity are available. The corresponding rain rates R are: level 1: $R < 0.25$ mm/h; level 2: $R < 12.5$ mm/h; level 3: $R < 25.0$ mm/h; level 4: $R < 50.0$ mm/h; level 5: $R < 125.0$ mm/h; level 6: $R > 125.0$ mm/h. Fig. 7 shows an image that was acquired by this C-band weather radar on September 22, 1996 at 0325 UTC, i.e., 1 minute after the acquisition of the SAR image depicted in Fig. 1. For better discrimination we have color-coded the six levels of rain rates. The circle segment inserted in the weather radar plot of Fig. 7 denotes its maximum range of 60 km. The box-marked area in this plot is the same as in the box-marked area in the SAR image (Fig. 1). For this area a detailed comparison of the rain rates derived from SAR image and the weather radar image will be carried out in Section VI.

Since this weather radar image was acquired quasisimultaneously with the ERS-2 SAR image, we may use it to compare

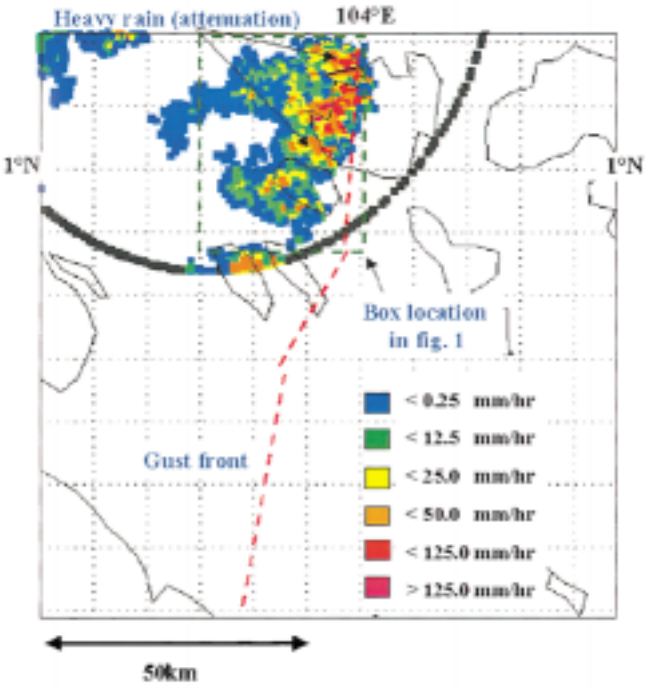

Fig. 7. Color-coded plot of radar reflectivity converted into rain rate derived from data of the C-band weather radar located in Singapore, which was acquired 1 min after the acquisition of the SAR image depicted in Fig. 1. The circle line denotes the maximum range of the radar. The imaged area contains the area of the SAR image depicted in Fig. 1 (box marked by a dashed line). Inserted is also the position of the gust front (red dashed line) visible on the SAR image (Fig. 1).

quantitatively the position of the gust front visible on the ERS-2 SAR image (Fig. 1) with the frontal line of the squall line visible on the weather radar image (Fig. 7). By comparing both im-

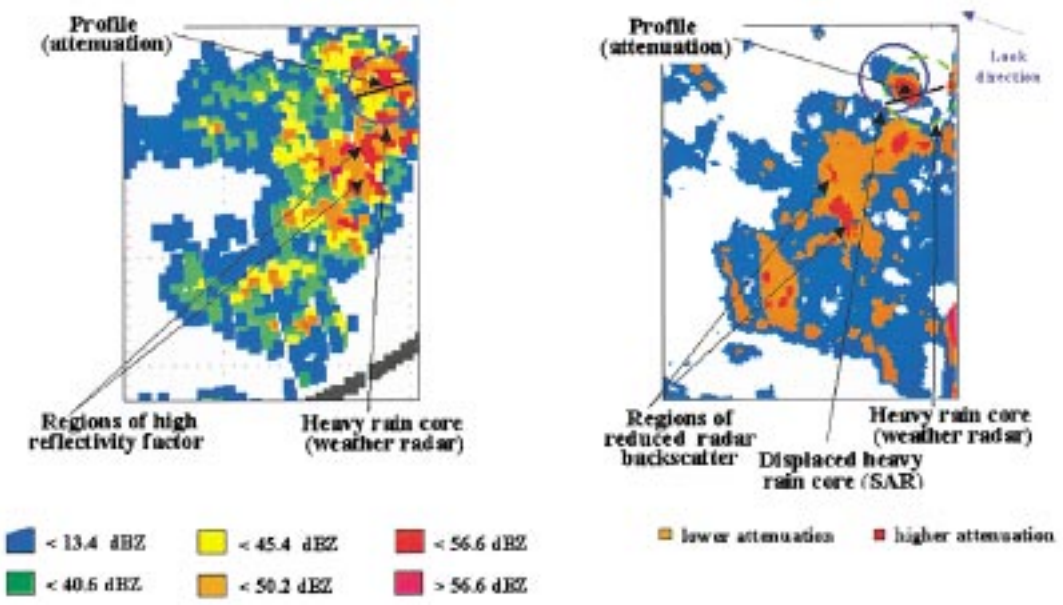

Fig. 8. Comparison of radar reflectivity as measured by the C-band weather radar with radar backscatter intensity extracted from the ERS-2 SAR image (right-hand plot) for the area which is box-marked in Figs. 1 and 7. The regions of high attenuation of the backscattered radar intensity by the rain drops in the atmosphere are well correlated with regions of high rain rate ($R > 50$ mm/h). The lines in the circled areas in the upper right-hand section of the plots denote the profile along which a quantitative comparison of the rain rate derived from the weather radar data and the ERS-2 SAR image is carried out.

ages we see that the gust front visible on the ERS-2 SAR image matches almost exactly with the front line of the squall line visible on the weather radar image. Furthermore, we note that the precipitation areas lie behind the gust front which is the interface between cold downdraft and warm ambient air. Furthermore, we see that the regions of high radar reflectivity in Fig. 7 corresponding to a high rain rate match well with the dark feature visible in the SAR image (Fig. 1). As the dark feature covers both land and sea, we interpret this as an indication that the radar backscatter is reduced by the attenuation of the rain column in the atmosphere. It is unlikely that it is caused by rain impinging on the sea surface or by wind effects, because the phenomenon is present over both land and sea as can be seen by comparing this SAR image with the one depicted in Fig. 2, which was acquired over the same area on a clear day. It can clearly be seen that much of the land area in Fig. 1 is obscured by the attenuation of the microwaves by the rain in the atmosphere.

Now we want to compare in more detail the ERS-2 SAR image of Fig. 1 with the S-band weather radar image depicted in Fig. 7. For this purpose we have taken the overlapping area marked by a box in Figs. 1 and 7 and have plotted in Fig. 8 the two subimages for better comparison color-coded side-by-side. We see that the regions of strong attenuation (strongly reduced radar backscatter) in the SAR image (right-hand image) correlate well with regions of high radar reflectivity (high dBZ values or high rain rates) in the weather radar image (left-hand image). We note that the regions of very strong attenuation are displaced in the radar look direction when compared with the weather radar image (left-hand image). This displacement is also indicative that the attenuated patterns originate from the rain column in the atmosphere. In this encircled area of Fig. 8 the displacement is measured to be 2 km.

Observing the rain band region (at the rear side of the gust front) in Fig. 1, we find regions with an inhomogeneous or mottled pattern. A possible explanation is that the squall line consists of many cells which may be at different stages of their life cycle (cumulus, mature, and dissipating stage), and thus are associated with different rainfall rates and wind gusts. These differences result in different radar backscattering and thus give rise to a mottled pattern in the SAR image. The exact mechanism, though, is a the combination of the effects from raindrops in the atmosphere (attenuation and volume scattering), raindrops impinging on the ocean surface (causing either an increase or decrease of the sea surface roughness), and roughening of the sea surface by downdrafts as discussed in Appendix B.

Immediately at the forefront of the gust front visible on the SAR image (Fig. 1) a dark region of reduced backscatter is found (Fig. 1). This feature is interpreted as a convergence zone in the windfield. At the rear side of the gust front, the downdraft wind is blowing toward the gust front, while at the fore side the ambient wind (from meteorological observation) is blowing against the gust front from the south-east direction. We may therefore conclude that there is a strong low level convergence of air which results in an absence of horizontal wind components. This interpretation is supported by the S-band weather radar image of 0400 UTC (Fig. 6). On this weather image new cells are visible in this convergence region. It is very likely that the strong upward motion of the convergent air induced convection favors the development of new cells. Indeed, in the weather radar image at 0500 UTC (not shown here), the cell structure is even more prominent.

VI. Estimation of Rain Rate

Now we want to extract quantitative rain rate information from the SAR image. For this purpose we have chosen a region where, according to the weather radar, the rain rate in some rain cores is very high ($>$ 125 mm/h). Such region is the encircled

area in the plots of Fig. 8. Along a profile in this heavy rain region (solid line in the encircled area) we have determined the variation of the NRCS in the SAR image and the variation of the reflectivity factor in the weather radar image. The variation of the NRCS is depicted in Fig. 9. It can be seen that in the center the NRCS decreases by more than 10 dB relative to the NRCS in the surrounding area. Using the weather radar image as a reference of the position of the rain core, this range displacement (d) can be used to calculate the effective thickness (h) of the rain column since

$$\frac{d}{h} = \tan(23.5^\circ) \tag{1}$$

where 23.5° is the incidence angle at this position in the ERS SAR scene. The displacement is found to be 2.0 km and the effective thickness of the rain core is thus given as $h = d/\tan(23.5^\circ) = 4.5$ km. The calculated effective thickness is then incorporated in the attenuation relationship for the rain rate estimation, which is adopted from [22]. In this paper, the attenuation relationship has been derived from data collected during typical rain events by using rain gauge and C-band weather radar from Darwin, Australia. The attenuation as a function of rain rate is given as

$$A = 0.0085 \times 2h \times R^{1.08} \tag{2}$$

where

A attenuate NRCS in decibels;
R rain rate in millimeters per hour;
h effective thickness of the rain column in km.

The effective thickness h is multiplied by two as the attenuation is two-ways. The attenuation A is calculated with reference to the NRCS of the neighboring no rain region. Using (2) we have inverted the NRCS values along the profile of Fig. 8 into rain rate. This rain rate, together with the one obtained from the weather radar along the same profile is plotted in Fig. 10. (Note that the reflectivity data were from the C-band weather radar binned in six discrete values.) It can be seen from this plot hat the two data sets are agreeable. Toward the two ends of the profile (corresponding to very low rain rate in weather radar), the attenuation-estimated rainfall rate is not valid since the attenuation effects is very small under such light rain condition.

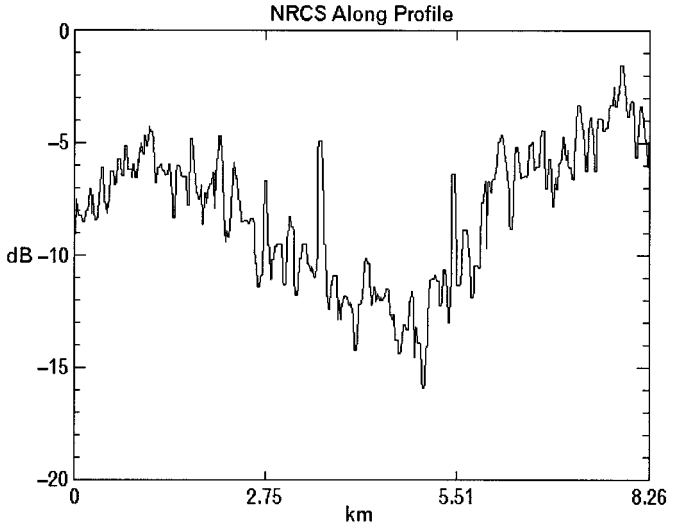

Fig. 9. Variation of the NRCS along the profile (line) inserted into the circle of the right-hand plot of Fig. 8.

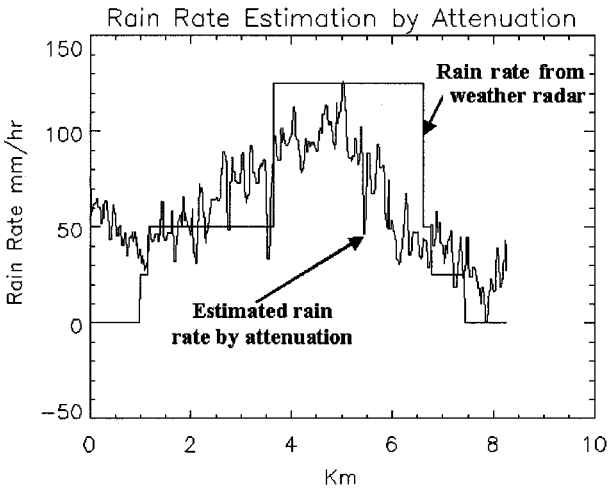

Fig. 10. Comparison between rain rate estimated by the radar reflectivity of the C-band weather radar and by the attenuation of the NRCS in the SAR image along the profile marked in Fig. 8. The discrete distribution of the rain rate derived from the weather radar data results from the fact that the whole range of rain rate is binned into six levels for data storage purpose.

VII. Estimation of Wind Speed

A conceptual meteorological model of a squall line is illustrated in Fig. 11 (adopted from [23]). At the rear of the gust front, air sloping downwards toward the gust front is observed. This information together with routine weather charts aid us in determining the wind direction. At the rear side of the gust front, the sea surface wind is blowing normal. After the determination of wind direction, the SAR image intensity is converted into NRCS and is averaged over 2 km for noise reduction. The effect of incidence angle across the range is also accounted for so that the wind speed will neither be overestimated at the near range nor underestimated at the far range [24]. The wind speed is then estimated using the inverse CMOD4 scatterometry model [20], [21]. The wind speed variation along the profile marked by a dotted line (from left to right) derived by this method is plotted in Fig. 12.

In general, wind-modulated NRCS exhibits uniform and gradual changes and the corresponding wind speed increases from around 3 to 6 m/s (Fig. 12). However, in the rain region (e.g., the mottled regions in Fig. 1), the scattering and attenuation effects of rain column from the atmosphere together with the effect of rain impinging on the ocean surface (see Appendix B) adds variability to the NRCS signature and thus to the wind speed. Such variability shows possible errors in wind speed estimation as part of the NRCS is caused by rain and not wind. Passing the gust front, the wind speed exhibits a sharp decrease. This region of sharp decrease is interpreted as a convergence zone in Section V where strong low level

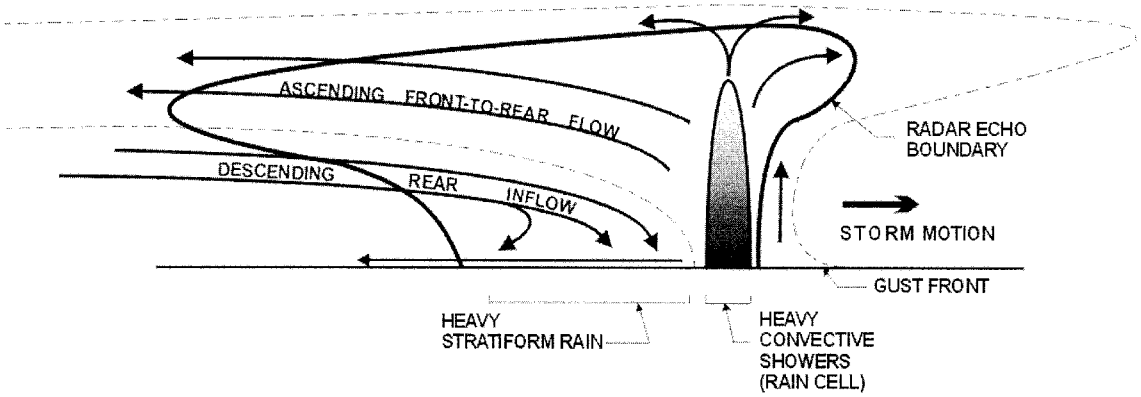

Fig. 11. Conceptual model of a squall line in a vertical cross section [adopted from Houze *et al.* (1989)].

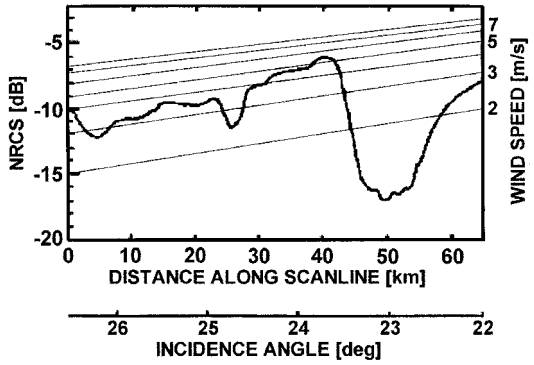

Fig. 12. Wind speed estimation using the CMOD 4 model along the profile marked by a dotted line in Fig. 1.

convergence of air results in the absence of a horizontal wind component.

VIII. Conclusions

In this paper, an ERS SAR image of a tropical squall line over coastal waters south of Singapore containing rain cores with very high rain rates (>100 mm/h) has been investigated. By comparing this ERS SAR image with weather radar images we conclude that the patterns visible on the SAR image indeed result from the squall line. The squall line was propagating southeastwards and the associated gust front and rain band is clearly seen in both weather radar and SAR images. In heavy rain areas (rain cores) with rain rates above 125 mm/h the attenuation of the 5.3 GHz (C-band) microwaves by the rain drops in the atmosphere is the dominant mechanism causing the radar signature of rain cells over ocean (and land) areas.

A region of reduced backscatter is observed immediately at the front edge of the gust front. This region is interpreted as a low level convergent area because such convergence induces convective activity which favors the generation of new cells. New cells are observed in the weather radar image approximately 30 minutes later which supports the above interpretation. Mottled image patterns associated with rain bands at the rear side of the gust front are observed. It is likely to be caused by the coexistence of old and new raincells where each cell has a different contribution to the backscatter signature. The SAR backscatter signature is further used to estimate the rain rate and wind speed associated with the squall line. It is found that the estimated rain rate in a region of heavy rainfall is consistent with the one obtained from the weather radar data. This suggests the possibility of deriving rain rates of tropical rain cells with high rain rates (>50 mm/h) from the SAR imagery. Possible errors in wind speed estimation due to rain effects are suggested. Future work involves further validation with ground truth data and error estimations.

Appendix A
Conversion of Radar Reflectivity Factor into Rain Rate

Weather radars measure the radar reflectivity caused by raindrops in the atmosphere. From the weather radar data a radar reflectivity factor is derived which depends on the raindrops size distribution [25], [26]. The reflectivity factor is then converted into rain rate (unit: mm/hour) by a relationship called Z–R relationship, which is written in the form

$$Z = aR^b$$

where

Z	radar reflectivity factor;
R	rain rate;
a and b	constants.

Unfortunately, there exists no universal Z–R relationship because it depends strongly on the type of rain. This is the reason why different authors have used different Z–R relationships for converting Z values into rain rates. The most widely used Z–R relationship is the Marshal–Palmer relationship with $a = 200$ and $b = 1.6$. Depending on the Z–R relationships used, the rain rate estimates may differ by more than 50% [Melsheimer, 1999, private communication].

APPENDIX B
PHYSICAL PROCESSES CAUSING RADAR SIGNATURES OF RAIN CELLS OVER OCEAN AREAS

Five different physical processes contribute to the radar signatures of rain cells visible on SAR images acquired over ocean areas [12], [27]–[36]: 1) attenuation and 2) scattering of the microwaves by the rain drops in the atmosphere, 3) increase of the sea surface roughness due to the generation of ring waves of the impinging rain drops, 4) decrease of the sea surface roughness due to the generation of turbulence in the upper water layer which dampens the water waves, and 5) roughening of the sea surface by wind gusts associated with rain cells. The scattering and attenuation of microwaves by rain drops (or more precisely: of hydrometeors) in the atmosphere has been extensively studied by radar meteorologists [25], [26]. For C-band radars operating at incidence angles between 20 and 80°, the radar backscattering at rain drops in the atmosphere is usually small compared to the radar backscattering at the sea surface. However, when the rain rate is above 50 mm/h the attenuation of C-band microwaves by rain drops in the atmosphere cannot be neglected [11] and can become the dominant effect when the rain rate is above 100 mm/h. This is the case in part of the rain area investigated in this paper.

In addition to the modification of the sea surface roughness by the impact of raindrops on the water surface, the sea surface roughness is also affected by the airflow associated with the rain event. Precipitation from a rain cell usually produces a downward airflow (downdraft) by entrainment and evaporative cooling under the cloud [2]. When the downdraft reaches the sea surface, it spreads radially outward as a strong local surface wind which increases the sea surface roughness. The outer edge of this airflow is called gust front. If the ambient wind field is weak and does not disturb this airflow pattern, the radially spreading downdraft is visible on SAR images of the sea surface as a nearly circular bright pattern with a sharp edge [4], [5]. However, when a strong ambient wind field is present, then the radially symmetric airflow pattern is distorted and the resulting radar signature is likewise distorted.

ACKNOWLEDGMENT

The authors would like to thank the Meteorological Service Singapore for providing the weather radar data. They would also like to thank C. Melsheimer, P. Brandt, and A. Michelsen of the Institute of Oceanography of the University of Hamburg, and J. Lu of the Centre for Remote Imaging, Sensing, and Processing, National University of Singapore, for their technical support.

REFERENCES

[1] P. S. Ray, Ed., *Mesoscale Meteorology and Forecasting*. Washington, DC: Amer. Meteorol. Soc., 1986.
[2] W. R. Cotton and R. A. Anthes, *Storm and Cloud Dynamics*. New York: Academic, 1989.
[3] L. L. Fu and B. Holt, "SEASAT views oceans and sea ice with synthetic-aperture radar," JPL Publ. 81-120, Jet Propul. Lab., Pasadena, CA, 1982.
[4] D. Atlas, "Footprints of storms on the sea: A review from spaceborne synthetic aperture radar," *J. Geophys. Res.*, vol. 99, pp. 7961–7969, 1994a.
[5] ——, "Origin of footprints on the sea seen by synthetic aperture radar," *Science*, vol. 266, pp. 1364–1366, 1994b.
[6] D. Atlas and G. Black, "The evolution of convective storms from their footprints on the sea as viewed by synthetic aperture radar from space," *Bull. Amer. Meteorol. Soc.*, vol. 75, pp. 1183–1190, 1994.
[7] T. Iguchi, D. Atlas, K. Okamoto, and A. Sumi, "Footprints of storms on the sea in the JERS-1 SAR image," *IEICE Trans. Commun.*, vol. E-78 B, pp. 1580–1584, 1995.
[8] J. Lichtenegger, "ERS-1 SAR images—Mirror of thunderstorms," *Earth Observ. Quart.*, no. 53, Sept. 1996.
[9] A. R. Jameson, F. K. Li, S. L. Durden, Z. S. Haddad, B. Holt, T. Fogarty, E. Im, and R. K. Moore, "SIR-C/X-SAR observations of rain storms," *Remote Sens. Environ.*, vol. 59, pp. 267–279, 1997.
[10] C. Melsheimer, W. Alpers, and M. Gade, "Investigation of multifrequency/multipolarization radar signatures of rain cells, derived from SIR-C/X-SAR data," in *Proc. Int. Geoscience and Remote Sensing Symp.*, Lincoln, NE, 1996.
[11] ——, "Investigation of multifrequency/multipolarization radar signatures of rain cells derived from SIR-C/X-SAR data," *J. Geophys. Res.*, vol. 103, pp. 18 867–18 884, 1998.
[12] ——, "Simultaneous observation of rain cells over the ocean by the synthetic aperture radar aboard the ERS-1/2 satellites and by weather radars," in *Proc. Int. Geoscience and Remote Sensing Symp.*, Hamburg, Germany, 1999, pp. 194–196.
[13] W. Alpers and B. Bruemmer, "Atmospheric boundary layer rolls observed by the synthetic aperture radar aboard the ERS-1 satellite," *J. Geophys. Res.*, pp. 12 613–12 621, 1994.
[14] P. W. Vachon, O. M. Johannessen, and J. A. Johannessen, "An ERS-1 synthetic aperture radar image of atmospheric lee waves," *J. Geophys. Res.*, vol. 99, no. C11, pp. 22 483–22 490, Nov. 15, 1994.
[15] W. Alpers and G. Stilke, "Observation of a nonlinear wave disturbance in the marine atmosphere by the synthetic aperture radar aboard the ERS-1 satellite," *J. Geophys. Res.*, vol. 101, pp. 6513–6525, 1996.
[16] C. Wackerman, C. L. Rufenach, R. A. Shuchman, J. A. Johannessen, and K. L. Davidson, "Wind vector retrieval using ERS-1 synthetic aperture radar imagery," *IEEE Trans. Geosci. Remote Sensing*, vol. 34, pp. 1343–1352, Nov. 1996.
[17] W. Alpers, U. Pahl, and G. Gross, "Katabatic wind fields in coastal areas studied by ERS-1 synthetic aperture radar imagery and numerical modeling," *J. Geophys. Res.*, vol. 103, pp. 7875–7886, 1998.
[18] S. Lehner, J. Horstmann, W. Koch, and W. Rosenthal, "Mesosccale wind measurements using recalibrated ERS SAR images," *J. Geophys. Res.*, vol. 103, pp. 7847–7856, 1998.
[19] G. Mueller, B. Bruemmer, and W. Alpers, "Roll convection within an arctic cold-air outbreak: Interpretation of *in situ* aircraft measurements and spaceborne SAR imagery by a three-dimensional atmospheric model," *Mon. Weather Rev.*, vol. 127, pp. 363–3809, 1999.
[20] A. Stoffelen and D. Anderson, "Characterization of ERS-1 scatterometer measurements and wind retrieval," in *Proc. 2nd ERS-1 Symp.—Space at the Service of Our Environment*, Hamburg, Germany, Oct. 1993.
[21] ——, "Scatterometer data interpretation: Estimation and validation of the transfer function CMOD4," *J. Geophys. Res.*, vol. 102, pp. 5767–5780, 1996.
[22] D. Atlas, D. Rosenfeld, and D. B. Wolff, "On C-band attenuation by tropical rainfall in Darwin, Australia using climatologically tuned Ze–R relations," in *3rd Int. Conf. Precipitation Modeling*. College Station, TX, Feb. 20–22, 1991.
[23] R. A. Houze, S. A. Rutledge, Jr., M. I. Biggerstaff, and B. F. Smull, "Interpretation of Doppler weather radar displays of midlatitude mesoscale convective systems," *Amer. Meteorol. Soc.*, vol. 70, no. 6, pp. 608–619, 1989.
[24] J. Horstmann, W. Koch, W. Rosenthal, and S. Lehner, "Wind fields from ERS SAR compared with a mesoscale atmospheric model near to the coast," in *Proc. 3rd ERS Symp.*, Florence, Italy, Mar. 17–21, 1997.
[25] R. J. Doviak and D. S. Zrnic, *Doppler Radar and Weather Observations*. New York: Academic, 1984.
[26] A. Sauvageot, *Radar Meteorology*. Norwood, MA: Artech House, 1991.
[27] R. K. Moore, Y. S. Yu, A. K. Fung, D. Kaneko, G. J. Dome, and R. E. Werp, "Preliminary study of rain effects on radar scattering from water surfaces," *IEEE J. Oceanic Eng.*, vol. 4, pp. 30–31, 1979.
[28] F. L. Bliven, P. Branger, P. Sobieski, and J. P. Giovanangeli, "An analysis of scatterometer returns from a water surface agitated by artificial rain: Evidence that ring waves are the main feature," *Int. J. Remote Sensing*, vol. 14, pp. 2315–2329, 1993.
[29] M. Tsimplis, "The effect of rain in calming the sea," *J. Phys. Oceanogr.*, vol. 22, pp. 404–412, 1992.
[30] Y. K. Poon, S. Tang, and J. Wu, "Interactions between rain and wind waves," *J. Phys. Oceanogr.*, vol. 22, pp. 976–987, 1992.

[31] F. L. Bliven and J. P. Giovanangeli, "An experimental study of microwave scattering from rain- and wind-roughened seas," *Int. J. Remote Sensing*, vol. 14, pp. 855–869, 1993.
[32] F. L. Bliven, P. Sobieski, and C. Craeye, "Rain generated ring-waves: Measurements and modeling for remote sensing," *Int. J. Remote Sensing*, vol. 18, pp. 221–228, 1997.
[33] C. Craeye, P. Sobieski, and F. L. Bliven, "Scattering by artificial wind and rain roughened water surfaces at oblique incidences," *Int. J. Remote Sensing*, vol. 18, pp. 2241–2246, 1997.
[34] P. W. Sobieski, C. Craeye, and L. F. Bliven, "Scatterometric signatures of multivariate drop impacts on fresh and salt water surfaces," *Int. J. Remote Sensing*, vol. 20, no. 11, pp. 2149–2166, 1999.
[35] N. Braun, M. Gade, and P. A. Lange, "Radar backscattering measurements of artificial rain impinging on a water surface at different wind speeds," in *Proc. Int. Geoscience and Remote Sensing Symp.*, Hamburg, Germany, 1999, pp. 200–202.
[36] J. Foerster, "On the action of rain in calming the sea and generating sea surface roughness," in *Proc. Int. Geoscience and Remote Sensing Symp.*, Hamburg, Germany, 1999, pp. 203–205.

I.-I. Lin received the B.Sc. degree from the Department of Atmospheric Science, National Taiwan University (NTU), Taipei, Taiwan, R.O.C., in 1989 and the Ph.D. degree in remote sensing from the University of Cambridge, Cambridge, U.K., in 1995.

From 1995 to 1999, she was a Research Scientist at the Center for Remote Imaging, Sensing, and Processing (CRISP), National University of Singapore. In 2000, she joined the National Center for Ocean Research (NCOR), NTU, where she is the Principal Investigator of the Remote Sensing Laboratory. Her research interests include applications of ocean color and hyperspectral remote sensing in the marine environment, multiple-sensor synergy, study of oceanic and atmospheric features over the ocean by using SAR imagery, and the study of severe weather systems (tropical storms, typhoons, and Mei-yu front) by remote sensing techniques, e.g., by scatterometers, SARs, and the sensors on board the TRMM satellite.

Werner Alpers (M'93) received the Dipl.-Phys. degree from the University of Hamburg, Hamburg, Germany, in 1962, the M.S. degree in physics from the University of Wisconsin, Madison, WI, in 1964, and the Ph.D. degree (Dr.rer.nat.) in theoretical physics (elementary particle physics) from the University of Hamburg in 1967.

He was with the European Space Research Institute (ESRIN), Frascati, Italy, from 1968 to 1970, where he worked in space physics. From 1970 to 1973, he was with the Max-Planck-Institute for Physics and Astrophysics, Munich, Germany. In 1973, he became engaged in remote sensing of the ocean and worked from 1973 to 1985 at the University of Hamburg and the Max-Planck-Institute for Meteorology, Hamburg. From 1985 to 1989 he was an Associate Professor at the Department of Physics and Electrical Engineering, University of Bremen, Bremen, Germany, and since 1989, he has been a Full Professor at the Institute of Oceanography, University of Hamburg, where he has been the Head of the research group "Satellite Oceanography." Currently, he is the Director of the Institute of Oceanography at the University of Hamburg. Since 1973, he has been engaged in microwave remote sensing of the ocean by using laboratory, airborne, and spaceborne sensors as well as theoretical models. He was a Principal Investigator for the Shuttle Imaging Radar B (SIR-B mission), and at present, he is a Principal Investigator for the ERS-1/2 and Shuttle Imaging Radar C/X-SAR missions. He has authored or coauthored more than 100 papers dealing with different aspects of microwave remote sensing of the ocean.

Dr. Alpers has been active in several advisory committees of the German Ministry of Science and Technology, the German Science Foundation, the European Space Science Foundation, and the European Space Agency (ESA) for defining earth observation satellite missions. In particular, from the beginning, he has been involved in the ERS-1, ERS-2, and Envisat satellite projects as an advisor to ESA.

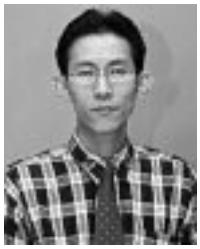

Victor Khoo Hock Soon received the B.S. degree in surveying (land) from the University of Technology, Malaysia, in 1994, and the M.S. degree in engineering from the Nanyang Technological University, Singapore, in 1997.

He is currently a Research Associate with the Surveying and Mapping Laboratory, School of Civil and Structural Engineering, Nanyang Technological University. From 1996 to 1998, he was an Associate Scientist with the Centre for Remote Imaging, Sensing and Processing (CRISP), National University of Singapore, Singapore. His research interests include GPS, GIS, and remote sensing.

Hock Lim (M'94) received the degree in physics from the University of Singapore, Singapore, and the Ph.D. degree in geophysical fluid dynamics from the University of Reading, Reading, U.K.

He was first a Meteorological Officer, and led the effort to computerize the operations of Meteorological Service Singapore in the early 1980s. There, he established the Laboratory for Image and Signal Processing in 1988, the Centre for Remote Imaging, Sensing and Processing (CRISP) in 1992, and coordinated the development of a computational science program from 1989 to 1993. He is currently Director of Temasek Laboratories, a newly established research institute in Singapore. His research interests include the dynamics of the atmosphere, image resolution, and remote sensing.

Tian Kuay Limreceived the B.Sc. degree (hons.) and the M.Sc. degree in physics, both from the National University of Singapore, Singapore, and has undergone postgraduate training in meteorology at the Bureau of Meteorology, Australia, and at Monash University, Australia.

He has been with the Meteorological Service of Singapore since 1985, where he is currently the Deputy Director (Science). He has developed and directed the implementation of various numerical models for the study of the tropical atmosphere, operational weather forecasting, and consultancy services for the aviation industry. In his current position, he oversees, organizes, and manages the department's resources, particularly in the use of science and technology, in the provision of meteorological services to meet the needs of aviation, shipping, specialized services, military operations, and the general public.

Dayalan Kasilingam (S'83–M'86) receievd the B.A. degree in electrical sciences from the University of Cambridge, Cambridge, U.K., in 1981, and the M.S.E.E. and Ph.D. degrees from the California Institute of Technology, Berkeley, in 1982 and 1987, respectively.

He is currently an Associate Professor of electrical and computer engineering with the University of Massachusetts, Dartmouth, and is on sabbatical at the U.S. Naval Research Laboratory, Washington, DC. He was the Senior Research Scientist with Ocean Research and Engineering, Pasadena, CA, where he developed numerous techniques for analyzing and retrieving information from SAR images of the ocean surface. From June 1996 to July 1997, he was with the Centre for Remote Imagin, Sensing, and Processing (CRISP), at the National University of Singapore, Singapore.

Dr. Kasilingam also served on the technical committees for the International Geoscience and Remote Sensing Symposium (IGARSS'97), Singapore, and the Progress in Electromagnetic Research Symposium (PIERS'00), Cambridge, MA. In 1995, he was awarded the Faculty Early Career Development Grant by the National Science Foundation.